J. Fluid Mech. (2005), *vol.* 542, *pp.* 139–164. © 2005 Cambridge University Press
doi:10.1017/S0022112005006324 Printed in the United Kingdom

Resonant interactions in rotating homogeneous three-dimensional turbulence

By QIAONING CHEN[1], SHIYI CHEN[1,2,3], GREGORY L. EYINK[1,3] AND DARRYL D. HOLM[4,5]

[1]Department of Mechanical Engineering, The Johns Hopkins University, Baltimore, MD 21218, USA

[2]CCSE and LTCS, Peking University, China

[3]Department of Applied Mathematics and Statistics, The Johns Hopkins University, Baltimore, MD 21218, USA

[4]Center for Nonlinear Studies and Theoretical Division, Los Alamos National Laboratory, Los Alamos, NM 87545, USA

[5]Mathematics Department, Imperial College London, SW7 2AZ, UK

(Received 30 March 2004 and in revised form 31 May 2005)

Direct numerical simulations of three-dimensional homogeneous turbulence under rapid rigid rotation are conducted for a fixed large Reynolds number and a sequence of decreasing Rossby numbers to examine the predictions of resonant wave theory. The theory states that 'slow modes' of the velocity, with zero wavenumber parallel to the rotation axis ($k_z = 0$), will decouple at first order from the remaining 'fast modes' and solve an autonomous system of two-dimensional Navier–Stokes equations for the horizontal velocity components, normal to the rotation axis, and a two-dimensional passive scalar equation for the vertical velocity component, parallel to the rotation axis. The Navier–Stokes equation for three-dimensional rotating turbulence is solved in a 128^3 mesh after being diagonalized via 'helical decomposition' into normal modes of the Coriolis term. A force supplies constant energy input at intermediate scales. To verify the theory, we set up a corresponding simulation for the two-dimensional Navier–Stokes equation and two-dimensional passive scalar equation to compare them with the slow-mode dynamics of the three-dimensional rotating turbulence. The simulation results reveal that there is a clear inverse energy cascade to the large scales, as predicted by two-dimensional Navier–Stokes equations for resonant interactions of slow modes. As the rotation rate increases, the vertically averaged horizontal velocity field from three-dimensional Navier–Stokes converges to the velocity field from two-dimensional Navier–Stokes, as measured by the energy in their difference field. Likewise, the vertically averaged vertical velocity from three-dimensional Navier–Stokes converges to a solution of the two-dimensional passive scalar equation. The slow-mode energy spectrum approaches $k_h^{-5/3}$, where k_h is the horizontal wavenumber, and, as in two dimensions, energy flux becomes closer to constant the greater the rotation rate. Furthermore, the energy flux directly into small wavenumbers in the $k_z = 0$ plane from non-resonant interactions decreases, while fast-mode energy concentrates closer to that plane. The simulations are consistent with an increasingly dominant role of resonant triads for more rapid rotation.

1. Introduction

Large-scale flows in oceans and the atmosphere are greatly affected by the Earth's rotation and are known to be quasi-two-dimensional. Rotation also plays an important role in many engineering flows, e.g. high-Reynolds-number turbulent flows in turbomachinery and rotating channels. When a fluid is under rotation, the Coriolis force is introduced into the momentum equation and competes with the nonlinear force. A dimensionless number, the Rossby number Ro, may be defined as the ratio of the magnitude of the inertial term to the Coriolis force. In a rapidly rotating fluid, a mathematical limit $Ro \to 0$ is taken of the three-dimensional Navier–Stokes equations. There is a general expectation that the fluid should become two-dimensional in this limit. For example, the classic Taylor–Proudman theorem implies that the Coriolis force will align vortex tubes parallel to the rotation axis in steady-state, rapidly rotating flows (Greenspan 1968).

To take into account the effect of rapid rotation on dynamical evolution a *resonant wave theory* has been applied (Greenspan 1968, 1969; Waleffe 1993). Similar theories were first developed for gravity waves in geophysical fluid flows (Phillips 1960) and have since been widely invoked elsewhere. For excellent reviews, see Phillips (1981) and Craik (1985). According to this approach, the fluid velocity may be regarded in the limit of small Rossby number as a superposition of inertial waves with a large characteristic frequency which are modulated on a longer, slow time scale. An averaged equation is derived from weakly nonlinear theory for the slow-time motion. This equation explains enhanced energy transfer from small scales to large scales by the resonant triadic interaction of inertial waves (Greenspan 1968, 1969; Waleffe 1993). Using an 'instability hypothesis', Waleffe (1993) argued further that resonant triadic interactions should drive the flow to become quasi-two-dimensional. More recently, this type of resonant wave theory has been put on a sounder mathematical footing. Embid & Majda (1996), Embid & Majda (1998) and Majda & Embid (1998) have derived similar 'averaged equations' in a rigorous asymptotic limit over a fixed time interval for a general class of geophysical fluids problems with fast wave dynamics. For the particular case of rotating incompressible fluids, it has been shown that the averaged equations contain as a subset the two-dimensional Navier–Stokes equations for the vertically averaged velocity fields (Mahalov & Zhou 1996; Babin, Mahalov & Nicolaenko 1996).

However, in *turbulent* flow under rapid rotation not only is the Rossby number Ro small, but also the Reynolds number Re is large. As a consequence, eddy motions are excited on a wide range of length scales. At any given wavenumber k there are thus at least two distinct time scales, the rotation time scale $\tau_\Omega \sim 1/(2\Omega)$ and the nonlinear time scale $\tau_{non}(k) \sim (k^3 E(k))^{-1/2}$ (where $E(k)$ is the energy spectrum). The validity of the wave resonance theories depends upon τ_Ω being shorter than all other time scales in the problem. However, for very large Reynolds numbers and for energy spectra decaying more slowly than k^{-3}, there will be a range of high wavenumbers k where instead $\tau_{non}(k) \ll \tau_\Omega$. Thus, the resonant wave theory is likely to be valid for turbulent flows only very non-uniformly in wavenumber, if at all. The existing mathematical derivations of the theory (Embid & Majda 1996, 1998; Majda & Embid 1998; Mahalov & Zhou 1996; Babin *et al.* 1996) are only usefully valid for low Reynolds numbers. Indeed, error fields for the resonant wave approximation are estimated in these proofs by 'Sobolev norms' that get most of their contribution from high wavenumbers. The errors are therefore shown, by present theorems, only to have upper bounds that grow rapidly with the Reynolds number Re. While the error bounds also decrease with Rossby number Ro, arguments based on comparing time scales,

like those above, suggest that resonant triads will be selected latest at the highest wavenumbers. Thus, very low Rossby numbers should be required in the existing proofs to guarantee that errors in the wave resonance theory are small for fully developed turbulent flow.

The present evidence from simulations and experiments is also mixed as to the regime of validity of the theory. Simulations of decaying rotating turbulence by Bardina, Ferziger & Rogallo (1985) showed a tendency for the length scales along the axis of rotation to grow as rotation rate increases. Bartello, Métais & Lesieur (1994) observed two-dimensional vortices emerging from the three-dimensional flow. Hossain (1994) showed that the turbulent flow reduced to an approximate two-dimensional state and the energy cascaded to longer length scales in a 32^3 forced simulation. These results are roughly in accord with the wave resonance theory. The first numerical work to study explicitly the relation of flow two-dimensionalization and resonant triadic interactions was Smith & Waleffe (1999). They observed a strong two-dimensionalization and a clear inverse energy cascade. However, they suggested that non-resonant interactions might still play an important role at rotation rates achieved in their simulations. So far the detailed predictions of two-dimensional turbulence theory have not been verified numerically in rotating three-dimensional turbulence and the role of resonant wave interactions has remained unclear for Reynolds number $Re \gg 1$. Thus, it is the purpose of this paper to investigate further the limit of rapidly rotating three-dimensional turbulence, where resonant interactions should dominate at leading order and two-dimensional turbulence be achieved.

The remainder of this paper is organized as follows. In § 2, we review the resonant wave theory of rapidly rotating fluids, including the rigorous mathematical results. In Appendix A we present, for completeness, a simple proof of Waleffe (1993) that vertically averaged or two-dimensional fields are not coupled to other modes by resonant triadic interactions. Particular attention will be paid to a 'Dynamic Taylor–Proudman theorem' that predicts the autonomous time-evolution of these two-dimensional fields. In Appendix B, we give an elementary derivation of this result based upon the 'averaged equation' of the resonant wave theory. In § 3, we discuss the numerical schemes and present our simulation results to investigate the mechanism of two-dimensionalization in rotating turbulence and to study the role of resonant triads. Finally, our conclusions are presented in § 4.

2. Resonant wave theory

Rapidly rotating fluids are a multi-time scale problem. In a rotating frame of reference, the Navier–Stokes equation reads (see Greenspan (1968))

$$\partial_t \boldsymbol{u} + 2\boldsymbol{\Omega} \times \boldsymbol{u} = -\nabla P/\rho + \nu \nabla^2 \boldsymbol{u} - \boldsymbol{\omega} \times \boldsymbol{u}. \tag{2.1}$$

Here, rotation vector $\boldsymbol{\Omega} = \Omega \widehat{\boldsymbol{z}}$. $\boldsymbol{u}(\boldsymbol{x})$ is the velocity field, $\boldsymbol{\omega} = \nabla \times \boldsymbol{u}$ is the vorticity field, ρ is the density, ν is the kinematic viscosity and P is the pressure in an inertial frame modified by a centrifugal term: $P = P_0 + \frac{1}{2}\rho \|\boldsymbol{\Omega} \times \boldsymbol{x}\|^2$. If L and U are characteristic length and velocity scales, then the above equation is non-dimensionalized as

$$\partial_{\tilde{t}} \tilde{\boldsymbol{u}} + \frac{2}{Ro} \widehat{\boldsymbol{z}} \times \tilde{\boldsymbol{u}} = -\tilde{\nabla} \tilde{P} + \frac{1}{Re} \tilde{\nabla}^2 \tilde{\boldsymbol{u}} - \tilde{\boldsymbol{\omega}} \times \tilde{\boldsymbol{u}}. \tag{2.2}$$

Here, Rossby number Ro is defined as

$$Ro = \frac{U}{\Omega L}, \tag{2.3}$$

and Reynolds number Re as

$$Re = \frac{UL}{\nu}. \tag{2.4}$$

For simplicity, we omit the symbol tilde from now on.

Naive perturbation theory or 'rapid-distortion theory' retains only the leading-order, fast linear dynamics in the limit $Ro \to 0$:

$$\partial_t \boldsymbol{u} + \frac{2}{Ro}\widehat{\boldsymbol{z}} \times \boldsymbol{u} = 0. \tag{2.5}$$

The solution of this equation is given by a superposition of *helical waves*:

$$\boldsymbol{u}(\boldsymbol{x}, t) = \sum_{\boldsymbol{k}} \sum_{s=\pm} a_s(\boldsymbol{k}, t)\boldsymbol{h}_s(\boldsymbol{k})\mathrm{e}^{\mathrm{i}\boldsymbol{k}\cdot\boldsymbol{x}} \tag{2.6}$$

where $\boldsymbol{h}_\pm(\boldsymbol{k})$ are the *helical modes*, defined as orthogonal eigenmodes of the curl operator, satisfying $\mathrm{i}\boldsymbol{k} \times \boldsymbol{h}_s = s|\boldsymbol{k}|\boldsymbol{h}_s$ with $s = \pm 1$ (Greenspan 1968; Waleffe 1992). The wave amplitudes exhibit fast harmonic oscillations $a_s(\boldsymbol{k}, t) = A_{s_k}\exp(\mathrm{i}\omega_{s_k} t/Ro)$ of frequency $\omega_{s_k} = 2s(\widehat{\boldsymbol{z}} \cdot \boldsymbol{k})/k = 2sk_z/k = 2s\cos\theta_k$, with θ_k the angle between $\boldsymbol{\Omega}$ and wavenumber vector $\boldsymbol{k}$. (As a convenient shorthand, we abbreviate the pair $(\boldsymbol{k}, s)$ as s_k.)

However, this naive perturbation theory is only asymptotically valid for very short times $t = O(Ro)$ as $Ro \to 0$, because it misses a slow, secular evolution of the wave amplitudes. That is, the solution of (2.2) evolves in fact on two distinct time scales, the slow time t and the fast time scale $\tau = t/Ro$ of the inertial waves. To leading order, this solution still takes the form of (2.6) but the wave amplitude satisfies a multiple-scale Ansatz $a_{s_k}(t, \tau) = A_{s_k}(t)\exp(\mathrm{i}\omega_{s_k}\tau)$, consisting of inertial waves with rapid oscillations on the fast time scale and amplitude $A_{s_k}(t)$ depending on the slow time t. This secular time-dependence can be obtained by substituting the helical mode expansion (2.6) into (2.2). On this basis, the Coriolis term is diagonalized and (2.2) takes the form

$$\left(\partial_t - \mathrm{i}\frac{1}{Ro}\omega_{s_k} + \frac{1}{Re}\,k^2\right)a_{s_k} = \frac{1}{2}\sum_{\boldsymbol{k}+\boldsymbol{p}+\boldsymbol{q}=0}\sum_{s_p, s_q} C_{\boldsymbol{kpq}}^{s_k, s_p, s_q} a_{s_p}^* a_{s_q}^*. \tag{2.7}$$

A standard multiple-scale asymptotic expansion is then made with $\partial_t \to \partial_t + (1/Ro)\partial_\tau$. The slow time-dependence of the amplitudes $A_{s_k}(t)$ is determined to eliminate secular terms growing like τ, yielding the 'averaged equation':

$$\left(\partial_t + \frac{1}{Re}\,k^2\right)A_{s_k} = \frac{1}{2}\sum_{\boldsymbol{k}+\boldsymbol{p}+\boldsymbol{q}=0}^{\omega_{s_p}+\omega_{s_q}+\omega_{s_k}=0}\sum_{s_p, s_q} C_{\boldsymbol{kpq}}^{s_k, s_p, s_q} A_{s_p}^* A_{s_q}^*, \tag{2.8}$$

valid for a slow time $t = O(1)$. Only 'resonant triads' satisfying

$$\omega_{s_p} + \omega_{s_q} + \omega_{s_k} = 0 \tag{2.9}$$

still remain in this equation. See Greenspan (1968); Waleffe (1993) for more details. Even higher-order asymptotic theories can be constructed, which have better accuracy for slow times $t = O(1)$ or which are asymptotically valid for even longer time intervals $t = O(1/Ro)$. For example, see Newell (1969). Such theories take into account near-resonances, in which the condition in (2.9) is not satisfied exactly but only to order $O(Ro)$, and higher-order resonances, such as resonant quartets in which four frequencies sum to zero. Such 'non-resonant effects' (by which we mean any interactions

other than from resonant triads) will be especially important at moderate Rossby numbers.

In the resonant wave theory there is a natural division of modes into two classes. The zero frequency modes or so-called *slow modes*, with $\omega_{s_k} = 0$, have $k_z = 0$ and thus coincide with two-dimensional modes having no variation along the rotation axis. The slow modes can also be obtained by vertically averaging the three-dimensional velocities

$$\overline{\boldsymbol{u}}^{3D}(x, y) = \frac{1}{H} \int_0^H \boldsymbol{u}(x, y, z)\, \mathrm{d}z,$$

with H the vertical height of the domain. The remaining modes with $k_z \neq 0$ are fully three-dimensional modes and, since they have non-zero frequency, are called *fast modes*. There are therefore three classes of resonant triads: 'fast-slow-fast' and 'slow-slow-slow' and 'fast-fast-fast'. We follow the convention that the first wavenumber in the triad is the one appearing on the left-hand side of equation (2.8), and is thus the mode which undergoes evolution due to interaction of the other two modes. For example, a 'fast-slow-fast' triad gives a contribution to the evolution of a fast mode due to the interaction of another fast mode and a slow mode. In such a resonant triad, the slow mode acts simply as a catalyst for energy exchange between the two fast modes and its own energy is unchanged (Greenspan 1969; Waleffe 1993). Formally speaking, there are resonant 'slow-fast-fast' triads, but they have zero coupling coefficient. Waleffe (1993) has shown this to hold for rapidly rotating three-dimensional flow as a consequence of the joint conservation of energy and helicity and, for the convenience of the reader, we reproduce his simple argument in Appendix A. This result is known to hold more generally in the theory of resonant fluid interactions, not only for simple rotation but also for β-plane flows (Longuet-Higgins & Gill 1967), stratified flows (Phillips 1968; LeLong & Riley 1991), rotating stratified flows (Bartello 1995), and rotating shallow-water flows (Warn 1986).

An important consequence is that the slow two-dimensional modes in the limit of rapid rotation evolve under their own autonomous dynamics. This consists of all the 'slow-slow-slow' triadic interactions, each of which is resonant. The averaged equation for the autonomous two-dimensional modes splits into two parts, as shown by Embid & Majda (1996) and Babin *et al.* (1996). As $Ro \to 0$, the vertically averaged horizontal velocity $\overline{\boldsymbol{u}}_H^{3D} = (\overline{u}^{3D}, \overline{v}^{3D})$ satisfies the two-dimensional Navier–Stokes (2D-NS) equation:

$$\partial_t \overline{\boldsymbol{u}}_H^{3D} + \left(\overline{\boldsymbol{u}}_H^{3D} \cdot \nabla\right) \overline{\boldsymbol{u}}_H^{3D} = -\nabla P_H/\rho + \nu \nabla^2 \overline{\boldsymbol{u}}_H^{3D}, \tag{2.10}$$

while the vertically averaged vertical velocity $\overline{w}^{3D}$ satisfies the two-dimensional passive scalar equation:

$$\partial_t \overline{w}^{3D} + \left(\overline{\boldsymbol{u}}_H^{3D} \cdot \nabla\right) \overline{w}^{3D} = \nu \nabla^2 \overline{w}^{3D}. \tag{2.11}$$

We give an elementary derivation of these results in Appendix B, assuming the validity of the averaged equation (2.8). Notice that it is not implied by this result that a flow under rapid rotation will become two-dimensional, but it does mean that the dynamics will contain an independent two-dimensional subdynamics, to leading order. In this respect, the result resembles the classic Taylor–Proudman theorem for steady flows (Greenspan 1968), so that it can be termed the 'Dynamic Taylor–Proudman Theorem.' Precisely, the statement is that the 'slow-slow-slow' triadic interactions yield the 2D-3C Navier–Stokes equations. 2D-3C means two variables (x,y) but three components $(\overline{u}^{3D}, \overline{v}^{3D}, \overline{w}^{3D})$.

The averaged equation (2.8) for the evolution of fully three-dimensional (fast) modes contains interactions of both the 'fast-slow-fast' and 'fast-fast-fast' types. While these cannot transfer energy directly to slow two-dimensional modes, Waleffe (1993) has argued that 'fast-fast-fast' resonances do play an important role in flow two-dimensionalization. As a consequence of an 'instability hypothesis', he has shown that energy in the fast three-dimensional modes is transferred by this set of resonances preferentially to slower modes, with smaller (but not zero) vertical wavenumber k_z. On the other hand, the catalytic 'fast-slow-fast' triads can transfer energy only between fast modes with the same wavevector magnitude k and the same value of $\cos\theta$ (Waleffe 1993). Hence, they can play no direct role in transferring energy between scales or in two-dimensionalization of the flow. Their plausible effect is simply to isotropize the fast mode energy distribution in the horizontal-wavenumber plane.

The multiple-scale Ansatz and the averaged equation (2.8) have been rigorously proved by Embid & Majda (1996) and Majda & Embid (1998) for a general fluid dynamical equation with fast wave dynamics, which includes rapidly rotating fluids as a special case. The precise statement of their result is that there exists some finite time $T > 0$ and an exponent $p > 1 + d/2$ (with d space dimensions) such that, for all $0 < t < T$,

$$\sum_{\boldsymbol{k},s_k} k^{2p} \left| a_{s_k}^{Ro}(t) - A_{s_k}(t) \exp(\mathrm{i}\omega_{s_k} t/Ro) \right|^2 = o(1) \tag{2.12}$$

as $Ro \to 0$, where $a_{s_k}^{Ro}(t)$ is the solution of the full equation (2.7) for given Rossby number Ro, and $A_{s_k}(t)$ is the solution of the averaged equation (2.8). Thus the error in the multiple-scale approximation goes to zero in the Sobolev-norm sense of (2.12) as $Ro \to 0$. This result can be stated in another way, in terms of the error field

$$\boldsymbol{\delta}^{Ro}(\boldsymbol{x}, t) \equiv \boldsymbol{u}^{Ro}(\boldsymbol{x}, t) - \boldsymbol{U}(\boldsymbol{x}; t, t/Ro), \tag{2.13}$$

where $\boldsymbol{u}^{Ro}(\boldsymbol{x}, t)$ is the solution of the rotating Navier–Stokes equation (2.2) and $\boldsymbol{U}(\boldsymbol{x}; t, \tau)$ is the multiple-scale Ansatz written in physical space. Define $E_\delta^{Ro}(k, t)$ as the wavenumber spectrum of the field $\boldsymbol{\delta}^{Ro}(\boldsymbol{x}, t)$, or the *error energy spectrum* (Kraichnan 1970; Leith & Kraichnan 1972). Then (2.12) is equivalent to the statement that, as $Ro \to 0$,

$$\int_0^\infty \mathrm{d}k \; k^{2p} E_\delta^{Ro}(k, t) = o(1), \tag{2.14}$$

for all $0 < t < T$ and some $p > 1 + d/2$. Thus, the theorem guarantees that some moment of the error spectrum goes to zero, at least over a finite time interval, as $Ro \to 0$.

The multiple-scale argument applies to any rotating three-dimensional flow, whether laminar or turbulent. However, the error bounds in (2.12) and (2.14) assume that, for $d = 3$, energy spectra decay faster than k^{-6} at high wavenumbers k, much steeper than turbulent spectra in the inertial range. Of course, when the Reynolds number Re is large but finite, then the spectra will eventually decay exponentially at large enough k, in the far dissipation range. However, because of the long inertial range, the Sobolev norms in (2.12) and (2.14) will become strongly Reynolds-number dependent, expected to grow as some power $(Re)^{\xi_p}$. Thus, the norms will not be small at high Reynolds number, except when the Rossby number is extremely low. Indeed, note that the spectral moments in (2.14) will get most of their contribution from near the Kolmogorov dissipation wavenumber k_d in a turbulent flow. That is the last wavenumber range where resonant triads will be selected as $Ro \to 0$, because the eddy turnover time $\tau_{non}(k_d)$ in the dissipation range is the shortest in the entire flow. Therefore,

Experiment/numerical simulations	Rossby number	Forcing scale
Traugott (1958) (decay)	$Ro^{\omega} = 1.65$	none
Wigeland & Nagib (1978) (decay)	$Ro^{\omega} = 0.4 \sim 16$	none
Bardina *et al.* (1985) (decay)	$Ro^{\omega} = 0.3 \sim 6.3$	none
Jacquin *et al.* (1990) (decay)	$Ro^{L} = 0.2 \sim 12$	none
Bartello *et al.* (1994) (decay)	$Ro^{\omega} = 0.01 \sim 100$	none
Hossain (1994) (forced)	$Ro^{L} = 0.1$	$11 \leqslant k_f^2 \leqslant 13$
Yeung & Zhou (1998) (forced)	$Ro^{L} = 0.00064 \sim 0.0195$	$k_f \leqslant 2$
Smith & Waleffe (1999) (forced)	$Ro^{L} = 0.17, 0.35$	$k_f = 24$
Our 128^3 DNS (2003) (forced)	$Ro^{L} = 0.0021 \sim 0.066$	$22 \leqslant k_f \leqslant 24$

TABLE 1. Different Rossby numbers from experimental and numerical studies.

the present theorems effectively say nothing about the validity of the resonant wave theory at high *Re*, for realistic values of the Rossby number. Since previous numerical simulations of rotating turbulence by Bardina *et al.* (1985), Bartello (1994), Mansour, Cambon & Speziale (1992), Hossain (1994), and Smith & Waleffe (1999) have also not verified the predictions of (2.8), its regime of validity for turbulent flow has remained unclear.

3. Numerical simulations and analysis

To address this issue, we have simulated the rotating Navier–Stokes equation (2.2) in a 128^3 periodic box with a forcing

$$f_i(\boldsymbol{k}, t) = \epsilon_{\boldsymbol{k},i} / \hat{u}_i(\boldsymbol{k}, t)^*. \tag{3.1}$$

Here, $\hat{u}_i(\boldsymbol{k}, t)^*$ is the conjugate of Fourier component $\hat{u}_i(\boldsymbol{k}, t)$. This force is specially chosen so that the energy input rates $\epsilon_{\boldsymbol{k},i}$ are all fixed (Siggia & Kerr 1978), and we choose the latter to be constant in a narrow band $22 < k_f < 24$ and zero elsewhere. Thus, the total input power $\epsilon = \sum_{\boldsymbol{k},i} \epsilon_{\boldsymbol{k},i}$ is constant, as are the separate energy inputs into slow modes and fast modes. This forcing guarantees also that the energy input is the same for all rotation rates. The normal viscosity term $\nu\nabla^2\boldsymbol{u}$ is replaced by a hyperviscosity term $(-1)^{q+1}\nu_q(\nabla)^{2q}\boldsymbol{u}$ with $q = 8$, to extend the inertial range. The Coriolis force and viscosity term are integrated exactly using a slaved, second-order Adams–Bashforth scheme. At each time step, the velocity in Fourier space $\hat{\boldsymbol{u}}(\boldsymbol{k}, t)$ is decomposed into the two helical modes and these two modes are evolved according to (2.7). The nonlinear term is calculated using the usual pseudospectral method and then projected onto the two helical modes (Smith & Waleffe 1999). The equation may be non-dimensionalized using the length scale $L_f = 1/k_f$ and velocity $U_f = (\varepsilon/k_f)^{1/3}$ from the forcing parameters. In that case, the dimensionless groups that appear are the forcing Rossby number (or macro-Rossby number) $Ro^L = (\epsilon k_f^2)^{1/3}/\Omega$ and a hyperviscous Reynolds number $Re_{(q)} = \varepsilon^{1/3}/(\nu_q k_f^{2(q-1/3)})$. In our simulations $Re_{(q)}$ was held fixed at 3260, while Ro^L was varied from 0.066 to 0.0021. Rossby numbers from the various experimental and numerical studies are collected in table 1. In the table *micro*-Rossby number $Ro^{\omega} = \omega'/(2\Omega)$ and ω' is r.m.s. vorticity.

Among the direct numerical simulations of forced rotating turbulence, Yeung & Zhou (1998) were interested in the dynamics in the range $k > k_f$, whereas we and others (Smith & Waleffe 1999; Hossain 1994) focus on the dynamics in the inverse

Type of triad	Resonant/Non-resonant	Characteristics as $Ro \to 0$
slow-slow-slow	R	2D+3C
slow-fast-fast	N	vanishing
fast-slow-fast	R + N	catalytic
fast-fast-fast	R + N	quasi-2D

TABLE 2. Triadic interactions in three-dimensional rotating turbulence.

energy cascade range $k < k_f$. We consider a transient flow state, in which rotation is begun after a statistically steady state is reached without rotation. The results shown below, if without specification, were obtained after taking an ensemble average over eight realizations started from distinct initial conditions. This simulation is patterned after a 128^2 simulation of two-dimensional N-S by Smith & Yakhot (1993). They found that an inertial-range energy spectrum $k^{-5/3}$ is established by the two-dimensional inverse cascade process and energy flux in the inverse cascade range is a negative constant, at least before energy begins to accumulate at the largest scales. To compare the results of our three-dimensional rotating simulation with its hypothetical limit, described by the 2D-NS and passive scalar equations, we carry out simultaneous calculations with (2.10) and (2.11) in which the initial conditions are the vertically averaged initial conditions of the rotating flow and the force is the vertically averaged three-dimensional force. In such a setup the simulation time is also the slow time t, in the notation of § 2. With these simulations we systematically check the main predictions of the averaged equation (2.8) for the resonant interactions.

As Rossby number asymptotically approaches zero, the resonant triadic interactions represented in the 'averaged equation' should become more and more dominant over the non-resonant ones. In table 2, all resonant and non-resonant triadic interactions and their characteristics in the rapid-rotation limit are listed. In this section, we examine carefully the validity of the resonant wave theory as we decrease the Rossby number. To be more specific, slow-slow-slow triadic interactions, slow-fast-fast triadic interactions and fast-fast-fast triadic interactions are studied, respectively.

3.1. *Energy spectra and transfer*

In figure 1 are plotted three-dimensional energy spectra for different Rossby numbers and also for the parallel two-dimensional run. In the plot, $k_h = (k_x^2 + k_y^2)^{1/2}$ is horizontal wavenumber magnitude. When rotation is 'turned on', energy is transferred to the large scales as shown in figures 1(a) and 1(c), consistent with the previous observations (Hossain 1994; Smith & Waleffe 1999). Notice that large-scale energy grows faster at $Ro = 0.066$ than at $Ro = 0.0021$, when the energy input is the same. For Rossby number $Ro = 0.17$, Smith & Waleffe (1999) observed a rapid energy transfer to low wavenumbers similar to ours at $Ro = 0.066$, which they interpreted as due to fast, non-resonant interactions of inertial waves. For both of our Rossby numbers, the flow tends to two-dimensionalize. In particular, figures 1(b) and (d) show that slow-mode energy $E(k_h, k_z = 0)$, energy from vertically averaged horizontal velocity $E_{uv}(k_h, k_z = 0)$ and total energy $E(k)$ all collapse together at large scales. This does not mean, however, that the fluid dynamics is that of 2D-NS. At $Ro = 0.066$, these three spectra are still far from the spectrum $E_{2D}(k_h)$ of the 2D-NS solution. It is only at our smallest Rossby number $Ro = 0.0021$ that the spectra of $k_z = 0$ modes begin to approach the two-dimensional-spectrum $E_{2D}(k_h)$ suggesting that the resonant wave theory is

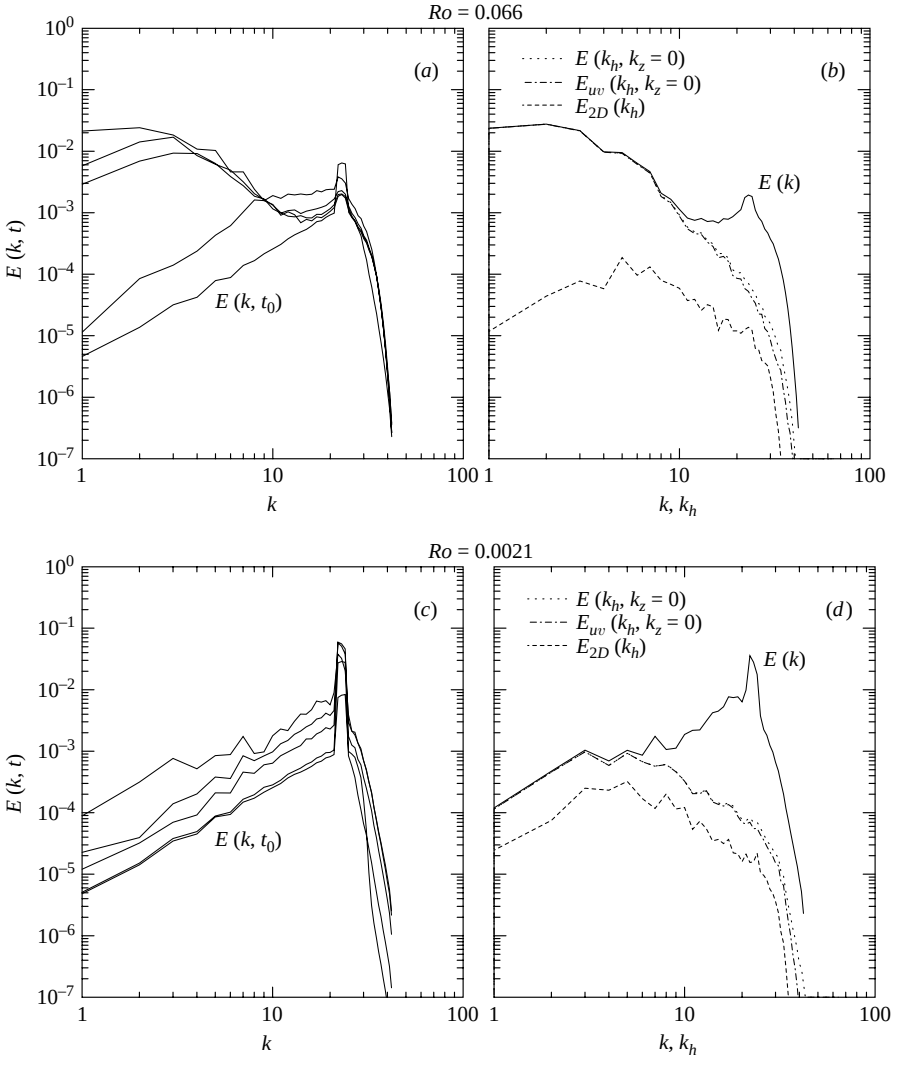

FIGURE 1. (*a*), (*c*) The time evolution of the energy spectrum for (*a*) $Ro = 0.066$ and (*c*) $Ro = 0.0021$ at $t = 0$, $t = 172\tau_0$, $t = 344\tau_0$, $t = 430\tau_0$ and $t = 600\tau_0$ (moving upward). Note that $E(k, t_0)$ is the initial energy spectrum and τ_0 is the initial large-eddy turnover time. (*b*), (*d*) Three types of spectra from one realization at time $t = 600\tau_0$ for (*b*) $Ro = 0.066$ and (*d*) for $Ro = 0.0021$.

becoming more valid. Even at $Ro = 0.0021$ the spectrum $E_{uv}(k_h, k_z = 0)$ plotted in figure 1(*d*) for time $t = 600\tau_0$ is nearly three times as large as $E_{2D}(k_h)$, due largely to a smaller energy input from the force into the two-dimensional flow.

To investigate how energy is transferred to the large scales, we calculate the energy transfer functions

$$T(k_h, k_z) = \sum_{S(k_h), I(k_z)} Re[\hat{\boldsymbol{u}}^* \cdot \hat{\boldsymbol{u}} \times \hat{\boldsymbol{\omega}}],$$

where $S(k_h)$ denotes a circular shell of horizontal wavenumbers with central radius k_h and $I(k_z)$ is an interval of vertical wavenumbers with midpoint k_z. These energy transfer functions are plotted for two rotation rates in figures 2 and 3, normalized by

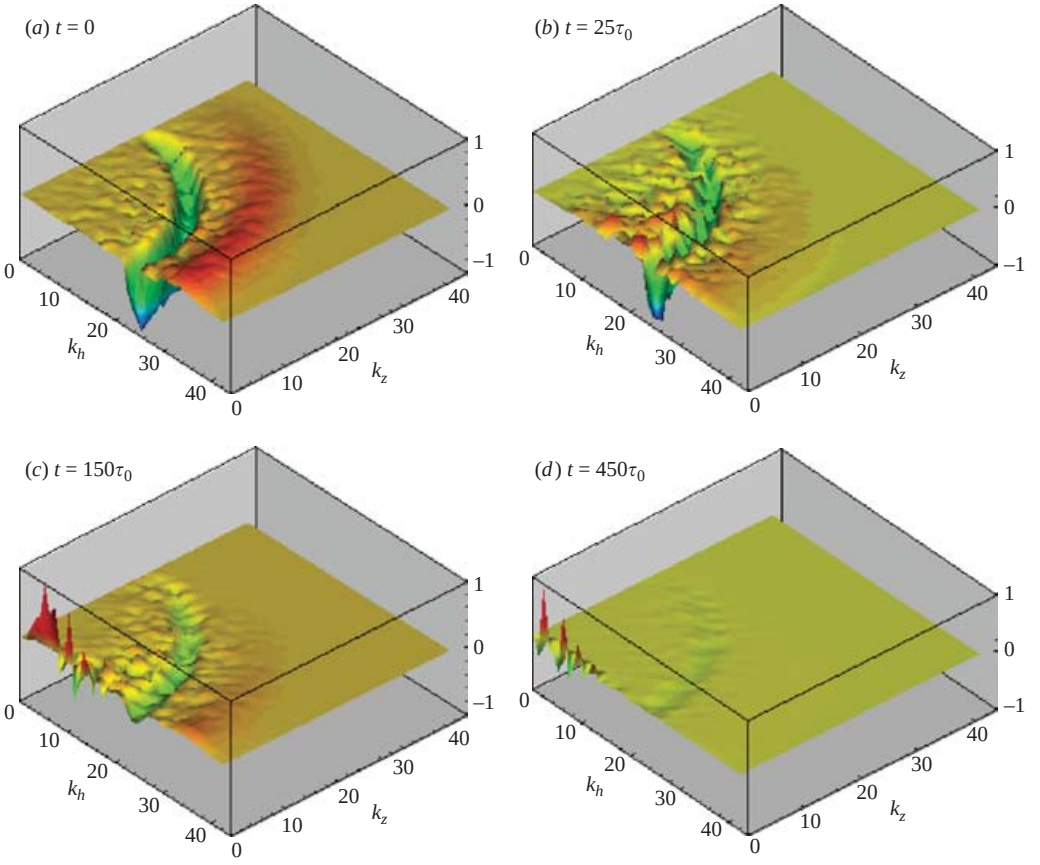

FIGURE 2. Normalized energy transfer functions $T(k_h, k_z)/|T|_{max}$ at different times for $Ro = 0.066$. The red colour indicates large positive transfer and the blue colour indicates large negative transfer. τ_0 is the initial large-eddy turnover time.

their largest absolute values. Initially, before rotation is added, most of the energy transfer activity happens in the vicinity of the forcing scale k_f, where $T(k_h, k_z)$ is negative (see figure 2*a*). The positive transfer at somewhat higher k represents a forward cascade of energy. When the system rotates slowly, at the largest simulated Rossby number $Ro = 0.066$, energy is quickly carried away from the forcing scales to the $k_z = 0$ plane, presumably by a combination of resonant and near-resonant interactions. This energy is then transferred further towards smaller k_h in the $k_z = 0$ plane (see figure 2), by essentially a two-dimensional inverse cascade. There is a general tendency, at all Rossby numbers, for the largest transfers at later times to be into the slow modes at $k_z = 0$. When the system rotates thirty times faster, at $Ro = 0.0021$ (see figure 3), the initial transfer is predominately from forward energy cascade. However, by $t = 450\tau_0$, most of the energy transfer is again concentrated near the $k_z = 0$ plane. If non-resonant interactions are largely suppressed at this Rossby number, then this transfer must arise from 'fast-fast-fast' resonances, as argued by Waleffe (1993). Even at this latest time hardly any transfer has developed in the $k_z = 0$ plane to smaller k_h, showing the two-dimensional inverse cascade is just incipient at this Rossby number.

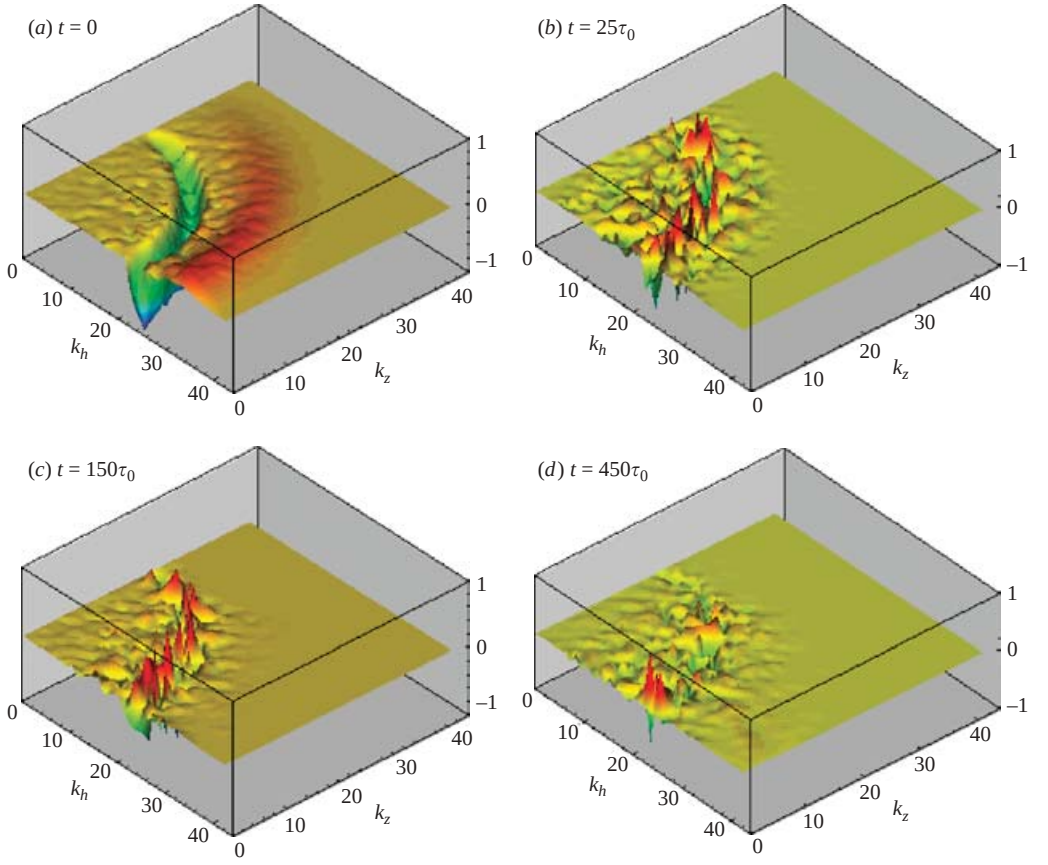

FIGURE 3. Normalized energy transfer functions $T(k_h, k_z)/|T|_{max}$ at different times for $Ro = 0.0021$.

3.2. *Dynamics of the slow modes*

The resonant wave theory predicts not just that two-dimensionalization will occur, but also that the slow two-dimensional modes will satisfy 2D-3C dynamics, and, in particular, should exhibit the phenomenology of the two-dimensional inverse cascade. To test this, we study the spectral transfer at various Rossby numbers. Energy is conserved for triads with all slow modes (since it is conserved in detail for all triads). Thus, we can define the energy flux

$$\prod_{sss}(k_h) = \int_{k_h}^{\infty} T_{sss}(k_h')\,\mathrm{d}k_h'$$

in horizontal wavenumber k_h, where the energy transfer function

$$T_{sss}(k_h) = \sum_{S(k_h)} Re[\hat{\boldsymbol{u}}_s^* \cdot \hat{\boldsymbol{u}}_s \times \hat{\boldsymbol{\omega}}_s]$$

only accounts for the contribution from slow modes. Note that the fields $\hat{\boldsymbol{u}}_s(\boldsymbol{k})$, $\hat{\boldsymbol{\omega}}_s(\boldsymbol{k})$ have been projected onto the subspace of slow modes, that is, they are set equal to $\hat{\boldsymbol{u}}(\boldsymbol{k})$, $\hat{\boldsymbol{\omega}}(\boldsymbol{k})$, respectively, on the $k_z = 0$ plane and zero elsewhere.† In figure 4 are plotted

† Equivalently, $\hat{\boldsymbol{u}}_s(\boldsymbol{k})$, $\hat{\boldsymbol{\omega}}_s(\boldsymbol{k})$ are just the three-dimensional Fourier transforms of the vertically averaged fields $\overline{\boldsymbol{u}}^{3D}(x, y)$, $\overline{\boldsymbol{\omega}}^{3D}(x, y)$.

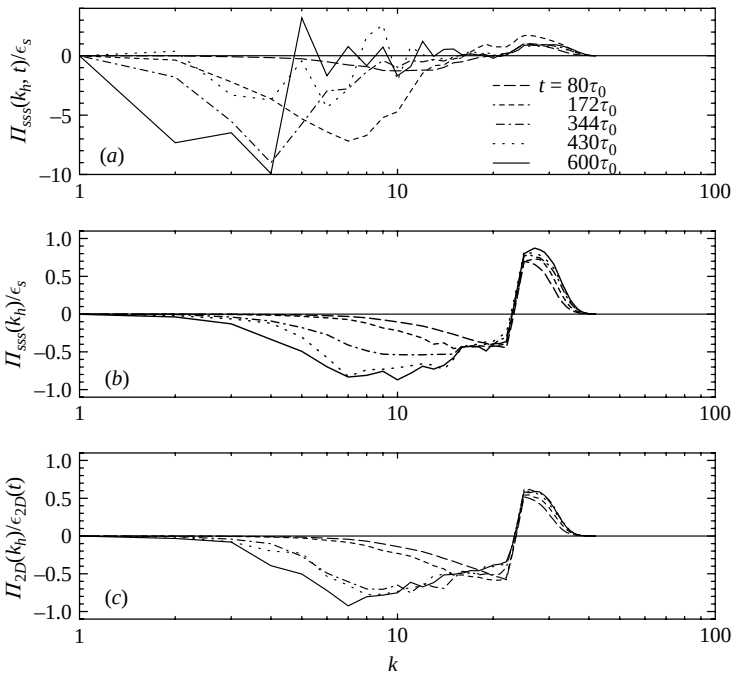

FIGURE 4. Normalized energy fluxes from slow-slow-slow interactions for (*a*) $Ro = 0.066$; (*b*) $Ro = 0.0021$; (*c*) normalized energy flux from two-dimensional Navier–Stokes at different times. Here, ϵ_s is slow-mode energy input for 3D-NS with rotation and $\epsilon_{2D}(t)$ is energy input for 2D-NS; τ_0 is the initial large-eddy turnover time. ϵ_s is the same for every rotation rate in our study.

energy fluxes $\Pi_{sss}(k_h)$ for different Rossby numbers together with the energy flux $\Pi_{2D}(k_h)$ from the corresponding two-dimensional simulation. At the larger Rossby number $Ro = 0.066$, energy fluxes not only fluctuate over time but also are much bigger than those at smaller Rossby numbers. At $Ro = 0.0021$, energy fluxes are negative at large scales showing a complete inverse energy cascade range. Moreover, around time $t = 400\tau_0$ the fluxes begin to develop a spectral range with constant value, as expected in two-dimensional turbulence, and in fact agree closely with those from 2D-NS (figure 4*c*). A consistent picture is obtained by fitting power laws to the energy spectra, at different rotation rates. figure 5(*a*) shows that slow-mode energy spectra $E(k_h, k_z = 0)$ are closer to k^{-3} than $k^{-5/3}$ at $Ro = 0.066$, in agreement with the findings of Smith & Waleffe (1999) at comparable Rossby numbers. However, at $Ro = 0.0021$ the spectrum scales as $k^{-5/3}$ (figure 5*b*) similar to that of the corresponding 2D-NS simulation in figure 5(*c*) and as expected for a transient two-dimensional inverse cascade with this forcing (Smith & Yakhot 1993).

In figure 6 we present at various Rossby numbers the time evolution of the energy spectrum $E_w(k_h, k_z = 0)$ of the vertically averaged vertical velocity $\overline{w}^{3D}$, compared with the time evolution of the spectrum $E_\theta(k_h)$ of a passive scalar in the two-dimensional parallel simulation. Figure 6(*a*) shows that at the highest simulated Rossby number $Ro = 0.066$ there is a tendency for an inverse cascade of $\overline{w}^{3D}$ towards the large scales. This is opposite to what happens for a passive scalar in a two-dimensional inverse energy cascade range, which is well known to experience a direct cascade to high wavenumber: see Celani *et al.* (2000) and our figure 6(*c*). However, as *Ro*

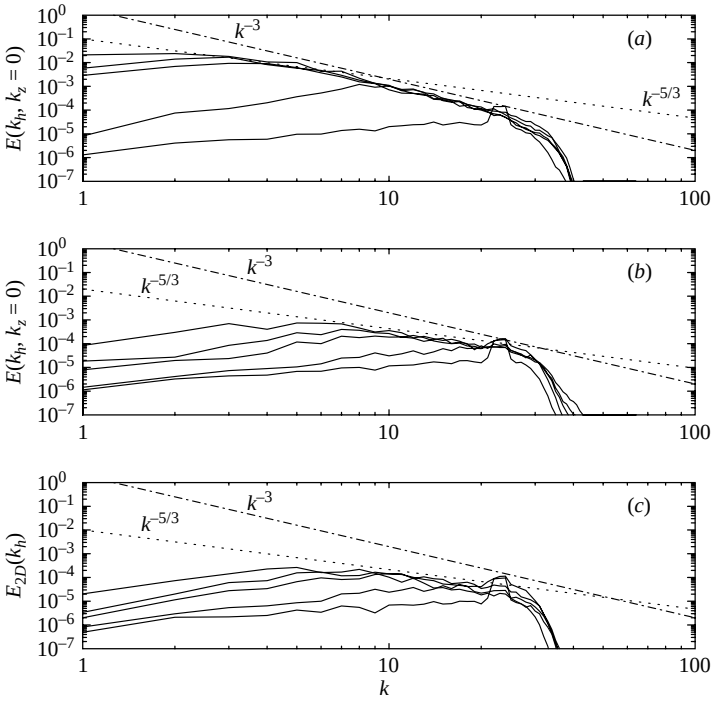

FIGURE 5. Time evolution of energy spectra (upward) from (*a*) slow modes at $Ro = 0.066$; (*b*) slow modes at $Ro = 0.0021$; (*c*) 2D-NS at $t = 80\tau_0$, $t = 172\tau_0$, $t = 344\tau_0$, $t = 430\tau_0$ and $t = 600\tau_0$.

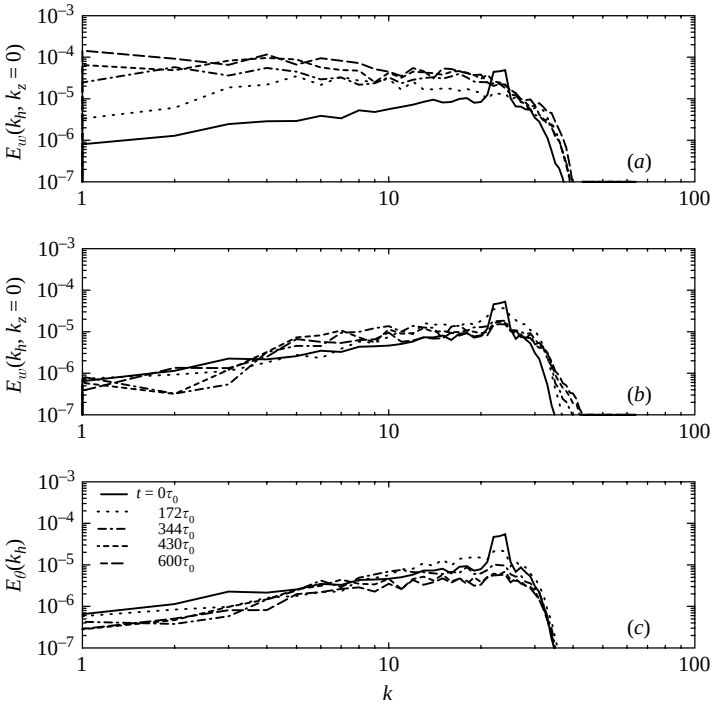

FIGURE 6. Time evolution of energy spectra (upward) of (*a*) $\overline{w}^{3D}$ at $Ro = 0.066$; (*b*) $\overline{w}^{3D}$ at $Ro = 0.0021$ and (*c*) two-dimensional passive scalar θ^{2D}.

decreases, the energy spectra of $\overline{w}^{3D}$ become closer to those of the two-dimensional passive scalar, especially at the lowest simulated Rossby number $Ro = 0.0021$ (see figure 6*b*). Thus, $\overline{w}^{3D}$ tends also to transfer downscale as the rotation rate increases.

The difference between the three-dimensional slow-mode dynamics and 2D-NS at finite Rossby numbers is also reflected in their different flow structures. In figures 7–9 are plotted the iso-surfaces of the vertically averaged vertical vorticity $\overline{\omega}_z^{3D}$ from the three-dimensional flow and those of the two-dimensional vorticity ω^{2D}. Here, the averaged vertical vorticity is

$$\overline{\omega}_z^{3D} = \frac{1}{H}\int_0^H \omega_z(x, y, z)\,\mathrm{d}z.$$

In figure 7 the formation of large vortices is seen at the higher Rossby number $Ro = 0.066$. Both cyclonic and anticyclonic vortices are present in the flow, which is different from the observations from Smith & Waleffe (1999).† Over the same time period, large vortices are not visible in the two-dimensional turbulent flow, which seems still in its infancy (see figure 9). However, at a much smaller Rossby number $Ro = 0.0021$, the flow structures at early times in three-dimensional bear a strong resemblance to those seen in two-dimensional (see figures 8 and figure 9, panels (*a*) and (*b*)). At later times the vortices in the smallest Rossby number three-dimensional flow are noticeably stronger than those in two-dimensional (figures 8 and 9, panels (*c*) and (*d*)).

The Dynamic Taylor–Proudman Theorem predicts that the three-dimensional slow modes will obey the 2D-3C Navier–Stokes equations, asymptotically for low Rossby numbers. As we discussed in the previous section (cf. (2.12), (2.14)), Embid & Majda (1996) and Majda & Embid (1998) measured the size of the deviations from this prediction by Sobolev norms of the error field with large p, which do not yield useful estimates for high-Reynolds-number flow. Therefore, we shall consider here instead $p = 0$, or the error energy itself, as in Kraichnan (1970) and Leith & Kraichnan (1972). It is useful to divide this error energy into separate contributions from horizontal and vertical velocity components. Precisely, we define

$$E_{\delta,H}(t) = \frac{1}{2}\int \mathrm{d}^2\boldsymbol{x}\left|\overline{\boldsymbol{u}}_H^{3D} - \boldsymbol{u}^{2D}\right|^2,\ \ E_{\delta,V}(t) = \frac{1}{2}\int \mathrm{d}^2\boldsymbol{x}\ |\overline{w}^{3D} - \theta^{2D}|^2. \tag{3.2}$$

As before, $\overline{\boldsymbol{u}}_H^{3D} = (\overline{u}^{3D}, \overline{v}^{3D})$ and $\overline{w}^{3D}$ are the vertically averaged horizontal and vertical velocities, respectively. For comparison, $\boldsymbol{u}^{2D} = (u^{2D}, v^{2D})$ is the solution of the 2D-NS equation (2.10) and θ^{2D} is the solution of the two-dimensional passive scalar equation (2.11). In figures 10(*a*) and 10(*b*) are shown the error energies in (3.2), normalized by the energies $E_H(t, Ro), E_V(t, Ro)$ of the corresponding three-dimensional vertically averaged fields, as functions of time at different Rossby numbers. Both plots show that the normalized error energy, at least over a finite interval of time, decreases as

† In their simulations, only cyclonic vortices were observed at larger Rossby numbers, as also in many geophysical flows. The only significant difference of our DNS from theirs at these Rossby numbers is the forcing, which was random (Gaussian, white-noise in time) in their case and deterministic (equation (3.1)) in ours. It is therefore tempting to suggest that our phase-coherent force acted to preserve the symmetry in the sign of vorticity of our initial conditions.

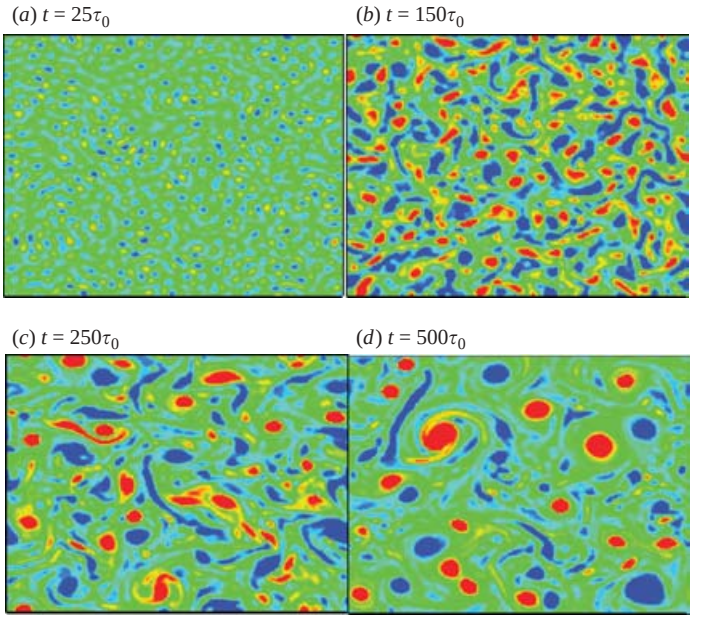

FIGURE 7. Time histories of the vertically averaged vertical vorticity $\overline{\omega}_z^{3D}$ iso-surfaces from three-dimensional rotating turbulence at $Ro = 0.066$. The red colour is for large positive vorticity and the blue is for large negative vorticity.

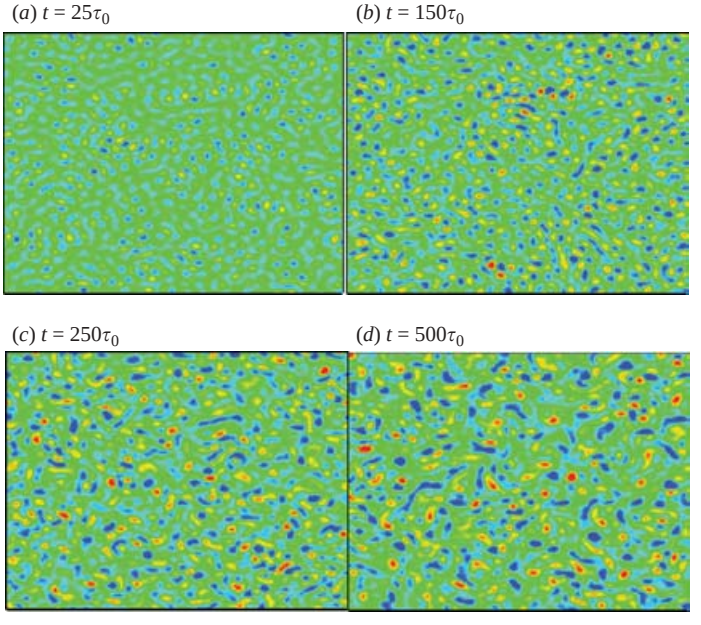

FIGURE 8. Time histories of the vertically averaged vertical vorticity $\overline{\omega}_z^{3D}$ iso-surfaces from three-dimensional rotating turbulence at $Ro = 0.0021$.

Rossby number is lowered. For any finite value of Ro, the vertically averaged three-dimensional solutions and the two-dimensional solutions begin to diverge as time t increases because of their chaotic dynamics and become uncorrelated, leading

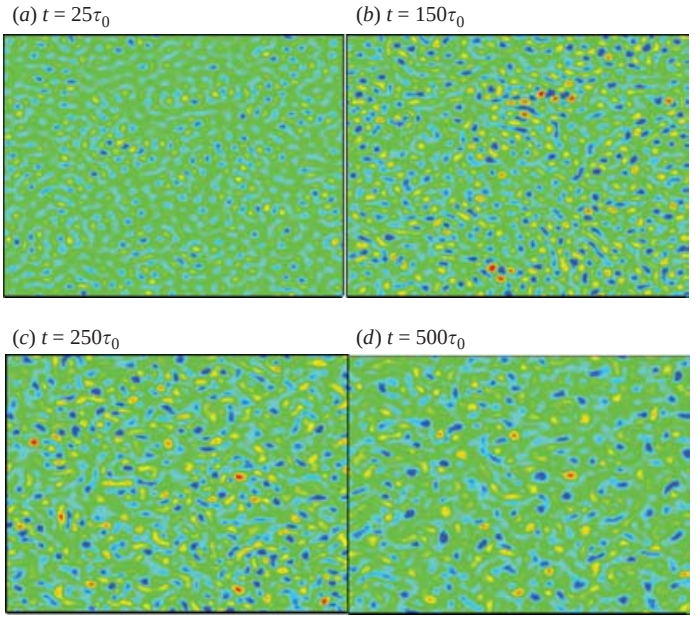

FIGURE 9. Time histories of the ω_z^{2D} vorticity iso-surfaces from 2D-NS.

to saturation of the normalized error energy at sufficiently long times.† Although presently available theorems do not rigorously imply the behaviour observed in figure 10 for the $p = 0$ norms, nevertheless these results are quite in line with expectations from the formal multi-time-scale analysis (Greenspan 1968; Waleffe 1993). For a range of slow time t the difference between the evolution of the vertically averaged fields under the full 3D-NS equation and under the averaged equation vanishes as the Rossby number tends to zero. At larger values of the slow time t the error arising from the averaged equation grows, implying non-resonant effects in the full three-dimensional solution. This is consistent with some recent closure theories, Cambon, Rubinstein & Godefred (2004), which predict coupling of slow and fast modes to higher-order accuracy or at longer times.

An important quantity to determine is the maximal length T_* of the slow-time interval over which the resonant wave theory becomes valid as $Ro \to 0$. The rigorous theorems guarantee that a finite time $T > 0$ exists so that Sobolev norms of the error (with $p > 1 + d/2$) converge to zero for all slow times $t \in [0, T]$. However, the asymptotic analysis does not determine the largest possible time T_* for which this is true. In order to estimate this, we have defined $T(Ro)$ for each Rossby number Ro as the time t for which the normalized error energy plotted in figure 10(a) first reaches the value 0.5. Beyond this time, non-resonant effects can certainly no longer be neglected. $T(Ro)$ is plotted as a function of Ro in figure 11. For a wide range of Rossby numbers above 0.00825, the graph can be fitted by a power law $Ro^{-1/2}$ with a small error bar (only 2%). The reason for such a power law to exist in this range is not clear. Interestingly, there appears to exist a transition when Rossby number is below 0.00825 and the slope of the graph decreases, perhaps even saturating to a

† Note that the saturation level is higher for the lower Rossby numbers, reversing the trend at early times. This seems to be due simply to our normalization of the error by the total energy and the fact that less energy has accumulated at a fixed time for lower Rossby numbers.

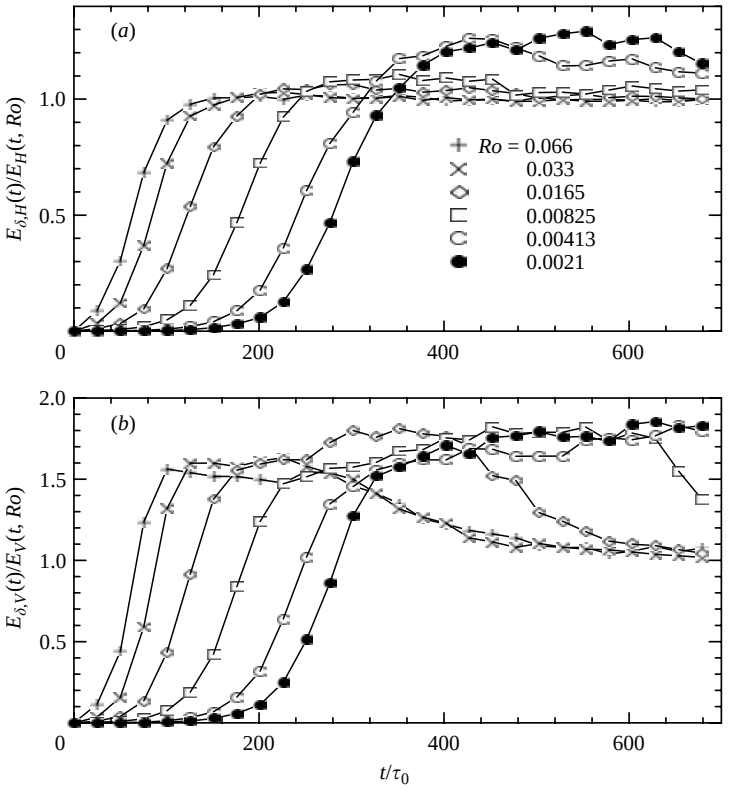

FIGURE 10. Normalized error energy for (*a*) $\overline{\boldsymbol{u}}_H^{3D} - \boldsymbol{u}^{2D}$ and (*b*) $\overline{w}^{3D} - \theta^{2D}$, as functions of time at different Rossby numbers. Here $E_H(t, Ro) = \frac{1}{2}\int |\overline{\boldsymbol{u}}_H^{3D}|^2$ and $E_V(t, Ro) = \frac{1}{2}\int |\overline{w}^{3D}|^2$.

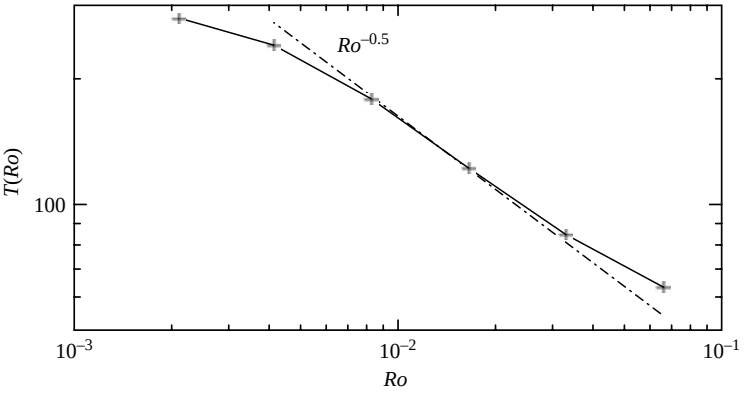

FIGURE 11. Time $T(Ro)$ vs. Rossby number Ro. There exists a power-law scaling $Ro^{-0.5}$ in the range $Ro > 0.00825$, but the graph appears possibly to platueau below $Ro = 0.00825$.

constant. If true, this implies that the resonant wave theory can be valid, even for arbitrarily small Ro, only in a finite time interval of length $< T_* = \lim_{Ro\to 0} T(Ro)$.

3.3. *Fast-mode interactions*

Our previous findings are consistent with the expected segregation of the autonomous two-dimensional slow modes from the three-dimensional fast modes to leading order at low Rossby numbers. All 'slow-fast-fast' triads transferring energy from a slow

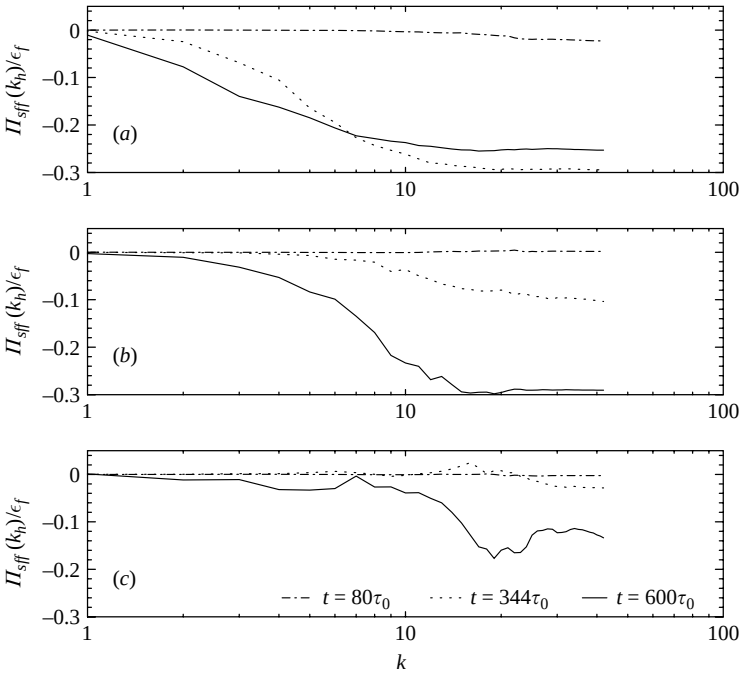

FIGURE 12. Normalized energy fluxes $\Pi_{sff}(k_h)$ from slow-fast-fast interactions for (*a*) $Ro = 0.066$; (*b*) $Ro = 0.00825$; (*c*) $Ro = 0.0021$ at different times. Here, ϵ_f is the total energy input into the fast three-dimensional modes.

mode by interactions with two fast modes are non-resonant and it is another main prediction of the resonant wave theory that such transfer should disappear as $Ro \to 0$. To test this, we calculate an energy flux into low-wavenumber slow modes from slow-fast-fast triadic interactions. Precisely, we define

$$\prod_{sff}(k_h) = -\int_0^{k_h} T_{sff}(k', k_z = 0)\,\mathrm{d}k'$$

where $T_{sff}(k_h, k_z = 0) = T(k_h, k_z = 0) - T_{sss}(k_h)$ is the energy transfer function from fast modes into slow modes at horizontal wavenumber k_h. Figure 12(*a–c*) shows that energy flux into slow modes at small k_h decreases as Ro decreases. In another words, less and less fast-mode energy is transferred into the large scales in the two-dimensional plane as $Ro \to 0$. At larger Rossby numbers, more energy is drained from fast modes directly into the large-scale slow modes by such non-resonant transfer, causing the flow to become two-dimensional more quickly than at smaller Rossby numbers. Smith & Waleffe (1999) suggested that this non-resonant mechanism was responsible for the rapid two-dimensionalization in their simulation at larger Rossby numbers.†

† Although we agree with their conclusion, we do not find the argument they offered very convincing. In their simulation, the forcing was white-noise in time with a wavenumber spectrum $F(k) = \epsilon_k \exp(-0.5(k - k_f)^2/\sigma^2)/\sqrt{2\pi\sigma^2}$, non-zero in a spherical shell with mean radius k_f and width σ. They attributed the strong two-dimensionalization they observed to non-resonant interactions, because of what they claimed was purely three-dimensional forcing. However, their forcing input energy not only into the fully three-dimensional modes but also into two-dimensional modes in the circular band where the spherical shell intersects the $k_z = 0$ plane. This energy will inverse cascade to large scales by 'slow-slow-slow' resonant interactions.

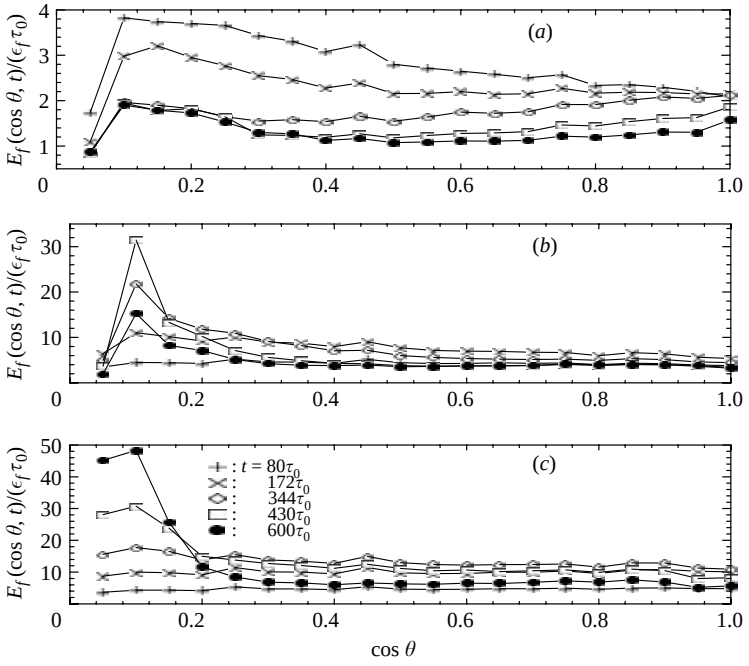

FIGURE 13. Normalized fast-mode energy distributions $E_f(\cos\theta, t)/(\epsilon_f\tau_0)$ for (*a*) $Ro = 0.066$; (*b*) $Ro = 0.00825$; (*c*) $Ro = 0.0021$ at different times.

A final prediction of the resonant wave theory is that, as $Ro \to 0$, fast-mode energy will tend to be transferred toward smaller values of $\cos\theta$ by 'fast-fast-fast' resonant interactions. Waleffe (1993) has demonstrated this tendency using the resonance condition (2.9) and a plausible 'instability hypothesis', which asserts that energy will tend to be transferred out from the unstable leg of a wavevector triad. Mansour *et al.* (1992) and Cambon & Jacquin (1989) have observed that energy was transferred towards small $\cos\theta$. However, neither distinguished fast modes from slow modes. Thus, the effects they saw may also be due to non-resonant transfer from fast modes directly into slow modes. In order to investigate the 'fast-fast-fast' interactions, we calculate the energy distribution $E_f(\cos\theta, t)$ only from fast modes. (We recall that the catalytic 'fast-slow-fast' interactions can only transfer energy between fast modes with the same value of $\cos\theta$ and thus cannot contribute to the dynamics of this quantity.) Figure 13(*a*) shows that $E_f(\cos\theta, t)$ flattens monotonically with time at the largest Rossby number $Ro = 0.066$, implying that fast modes behave largely three-dimensionally. At the middle Rossby number $Ro = 0.00825$ (figure 13*b*), $E_f(\cos\theta, t)$ peaks at smaller $\cos\theta$ at earlier times and then flattens everywhere at later times. However, at the smallest Rossby number $Ro = 0.0021$, fast-mode energy monotonically builds up at small $\cos\theta$ (figure 13*c*). Assuming that resonant interactions dominate at that Rossby number, this observation supports the conclusions of Waleffe (1993) based on the 'instability hypothesis'.

4. Conclusions

To summarize briefly our results, this is the first numerical simulation of forced homogeneous rotating turbulence to explore quantitatively the long-time effects of resonant interactions on the two-dimensionalization as $Ro \to 0$. We have accomplished

this by a systematic study of the fluid velocity field decomposed into 'slow' (two-dimensional) modes and 'fast' modes. We demonstrate an inverse cascade regime for the slow modes with the characteristics of two-dimensional turbulence, namely, a $k_h^{-5/3}$ spectral range where energy flux is negative and constant for the slow-mode dynamics (figures 4 and 5). This is consistent with the predictions of 2D-3C equations, corresponding to resonant interactions. Three additional findings verify the increasing importance of resonant interactions to two-dimensionalization at small Ro. First, vertically averaged three-dimensional velocities ($\overline{u}^{3D}, \overline{v}^{3D}, \overline{w}^{3D}$) and the solutions of 2D-3C equations converge as $Ro \to 0$, in the sense that the energy in their difference fields vanishes (figure 10). Second, non-resonant energy flux into small k_h in the $k_z = 0$ plane from slow-fast-fast triads decreases as Ro decreases (figure 12). Finally, fast-mode energy is transferred toward the $k_z = 0$ plane, consistent with the prediction of Waleffe (1993) that resonant interactions of fast modes drive the flow to become quasi-two-dimensional (figure 13).

Our work has a couple of limitations that it would be interesting to overcome in future investigations.

First, our main concern has been to study rotating fluid turbulence for both high Reynolds number Re and low Rossby number Ro. The approach of this initial study has been to simulate a single large Reynolds number for a sequence of decreasing Rossby numbers. It would be more informative to vary both parameters and to map out the behaviour for a sequence of increasing Reynolds numbers as well. Of course, this will require increasing grid resolution for the DNS and it is computationally challenging, given the multiple time scales involved in rapidly rotating flow. In principle, our conclusions could change, at least quantitatively, at higher Reynolds numbers. Note that increasing the grid resolution also increases the wavenumber mode density and, thus, the number of resonances and near-resonances. Likewise, altering the aspect ratio of the flow domain may either increase or decrease the number of resonant triads available. It is possible that changing the number of such resonances could modify their effect. On the other hand, exact resonances even in the limit of continuous wavenumbers are a codimension-1 subspace of the set of all triads and always represent a relatively small fraction of the triadic interactions. It is precisely this reduction in the number of effective interactions that provides hope for a simpler description of rapidly rotating turbulence.

A second limitation of our study is that we have not always separated cleanly resonant and non-resonant effects. Thus, in our analysis of 'slow-fast-fast' transfer (figure 12), we could say with certainty that this is due to non-resonant interactions, because resonant 'slow-fast-fast' triads have zero coupling coefficient (Appendix A). However, in our study of 'fast-fast-fast' transfer in the same subsection (figure 13), we did not disentangle the distinct contributions of resonant and non-resonant interactions. To do so would require simulating the full 'averaged equation' (2.8) summing over all resonant triads. We have learned that equation (2.8) has in fact recently been simulated, but at a somewhat lower resolution of 64^3 than our DNS, by Y. Lee & L. M. Smith (2004, personal communication). Carrying out such a study at higher resolutions is an important goal for future research. This is difficult because it involves a complete enumeration of all such triple resonances and also because the nonlinearity in equation (2.8) is not of convolution type and can no longer be calculated efficiently in physical space via FFT. We simulated instead a subset of the averaged equation (2.8), namely, the autonomous set, (2.10) and (2.11), satisfied by the 'slow' two-dimensional modes. These equations describe the effects of the 'slow-slow-slow' triads, which are all resonant.

Our work has investigated rapidly rotating turbulent fluids as a case study in the application of resonant wave theory. The results of the study therefore have more general interest than for this particular problem. The same type of theory has been widely applied to geophysical turbulent flows with rotation and/or stratification (Phillips 1981; Craik 1985). Details of the predictions may differ considerably according to the context. For example, Bartello (1995) used a similar reasoning as that of Waleffe (1993) to argue that for rotating, stratified turbulence the catalytic, 'fast-slow-fast' resonant triads will transfer the energy in fast gravity waves downscale and provide a primary mechanism of nonlinear geostrophic adjustment, while the 'fast-fast-fast' resonant interactions will be of secondary importance. In rapidly rotating fluids without density stratification, we find that the opposite is true. Nevertheless, many of the basic issues are the same in all applications of the resonant wave theory to high-Reynolds-number turbulent flows. Therefore, it may be useful to summarize several key conclusions from our investigation of this one example.

First, the main predictions of the wave-resonance theory appear to hold for $Ro \ll 1$ and $Re \gg 1$ simultaneously (as outlined in the opening paragraph of this section). Convergence of the approximation holds in the useful sense that the energy in the error fields decreases to zero, over a finite time interval. Present rigorous theorems (Embid & Majda 1996, 1998; Majda & Embid 1998) use Sobolev-norm estimates that yield useful estimates for rotating laminar flows, but not for fully developed turbulence. An optimistic conclusion of our work is that those theorems can probably be improved, by substitution of an L^2 or energy norm for the Sobolev norms. A proof of this may not be easy, given the current lack of understanding of the inviscid, high-Reynolds-number limit of fluid equations. However, our numerical results lend support to the idea that the energy-containing, large-scale motions in turbulent flow will conform to the predictions of resonant wave theory in the appropriate limit.

We find that there is an intrinsic time restriction on the validity of the resonant wave theory. The formal multiple-scale analysis, as well as the rigorous theorems, predict that there should be a finite interval of the slow-time variable t over which the approximation will converge. They do not answer the question whether this time interval is finite in fact, or whether the approximation will be valid at any arbitrary time for a sufficiently small Rossby number. Our numerical results seem to indicate either that the convergence holds over only a finite time interval or else that the Rossby numbers required for a close approximation become extremely small beyond a certain time horizon. Of course, both the dynamics involved – rotating 3D-NS (2.2) and the low-Rossby-number limiting dynamics given by the averaged equation (2.8) – are chaotic at high Reynolds number and a rapid exponential divergence of their solutions is to be expected for finite Ro. This does not imply a necessary failure of the resonant wave theory applied to forced, statistically stationary turbulence, since chaotic dynamics often possess 'structural stability' of their long-time statistics.

A more serious limitation of the wave resonance theory may be the magnitude of the Rossby numbers required for convergence, even at relatively early times. We have found sizable non-resonant effects for Rossby numbers as small as $Ro = 0.066$. Since the Rossby number is not extremely small in most engineering applications, flow two-dimensionalization is there probably due mainly to the non-resonant interactions, for which the two-dimensional dynamics is not segregated from the three-dimensional dynamics. However, the resonant wave theory provides the correct 'rapid-distortion limit' for fast rotations. Therefore, it may still be useful to take into account the resonance conditions in statistical modelling schemes for engineering purposes, as a constraint which becomes exact as $Ro \to 0$. Resonant interactions may be more

important for geophysical flows, where typical Rossby numbers are much smaller. However, for the atmosphere at midlatitude synoptic scales, the typical Rossby number is only about $Ro = 0.1$ and even for the Gulf Stream with smaller characteristic velocities the Rossby number is only $Ro = 0.07$ (Pedlosky 1987). In our simulations, this is a marginal value to observe the predictions of the theory. A combination of rotation with other effects such as stratification may be necessary in the atmosphere and oceans to select resonant interactions of fast waves.

Direct numerical simulations are performed in LSSC-II at the State Key Laboratory on Scientific and Engineering Computing in China and at the cluster computer supported by NSF Grant No. CTS-0079674 at the Johns Hopkins University.

Appendix A. Decoupling of the slow two-dimensional modes

An important result mentioned in the text is that there is zero coupling constant for resonant 'slow-fast-fast' triads in an incompressible fluid subjected to rapid rigid rotation. This implies that the 'slow' two-dimensional modes evolve independently of the 'fast' modes through the leading-order resonant interactions, in the limit of small Rossby numbers. This result was derived first by Greenspan (1969) for eigenmodes in a bounded container and later by Waleffe (1992) using detailed conservation of both energy and helicity on a basis of helical plane waves. For the convenience of readers, we reproduce here Waleffe's simple and elegant demonstration.

The coupling constant that appears in the Navier–Stokes equation expressed by helical modes, (2.7), was shown by Waleffe (1992) to have the form

$$C_{\boldsymbol{kpq}}^{s_k,s_p,s_q} = \tfrac{1}{2}(s_p p - s_q q)\boldsymbol{h}_{s_p}^* \times \boldsymbol{h}_{s_q}^* \cdot \boldsymbol{h}_{s_k}^*, \tag{A 1}$$

with notational following that in our § 2. This coupling constant satisfies the joint constraints of detailed energy conservation

$$C_{\boldsymbol{kpq}}^{s_k,s_p,s_q} + C_{\boldsymbol{pqk}}^{s_p,s_q,s_k} + C_{\boldsymbol{qkp}}^{s_q,s_k,s_p} = 0 \tag{A 2}$$

and of detailed helicity conservation

$$s_k k C_{\boldsymbol{kpq}}^{s_k,s_p,s_q} + s_p p C_{\boldsymbol{pqk}}^{s_p,s_q,s_k} + s_q q C_{\boldsymbol{qkp}}^{s_q,s_k,s_p} = 0 \tag{A 3}$$

for all triads of helical modes. These two constraints may be expressed equivalently by the following equality of ratios:

$$\frac{C_{\boldsymbol{kpq}}^{s_k,s_p,s_q}}{s_q q - s_p p} = \frac{C_{\boldsymbol{pqk}}^{s_p,s_q,s_k}}{s_k k - s_q q} = \frac{C_{\boldsymbol{qkp}}^{s_q,s_k,s_p}}{s_p p - s_k k}. \tag{A 4}$$

The key point in Waleffe's argument is to compare the latter relation with a similar one derived from the resonance condition, (2.9) in the text, or $\omega_{s_p} + \omega_{s_q} + \omega_{s_k} = 0$. After substituting the dispersion relation for helical waves $\omega_{s_k} = 2s\cos\theta_k$, this becomes

$$s_k \cos\theta_k + s_p \cos\theta_p + s_q \cos\theta_q = 0. \tag{A 5}$$

Projecting the wavenumber triad condition $\boldsymbol{k} + \boldsymbol{q} + \boldsymbol{p} = 0$ onto the rotation axis gives another equation

$$k\cos\theta_k + p\cos\theta_p + q\cos\theta_q = 0. \tag{A 6}$$

In the same way as for the coupling constants, (A 5) and (A 6) together are equivalent to an equality of ratios:

$$\frac{\cos\theta_k}{s_p q - s_q p} = \frac{\cos\theta_p}{s_q k - s_k q} = \frac{\cos\theta_q}{s_k p - s_p k}, \tag{A 7}$$

valid for any resonant triad. Comparing (A 4) and (A 7) immediately yields the main result. Indeed, s_q is a slow mode if and only if $\cos\theta_q = 0$. Suppose, then, that s_q is a slow mode and s_k, s_p are fast modes. Equations (A 4) and (A 7) imply that $C_{\boldsymbol{kpq}}^{s_k,s_p,s_q}$ stands in the same ratio to $C_{\boldsymbol{kpq}}^{s_k,s_p,s_q}$, say, as $\cos\theta_q$ does to $\cos\theta_k$. Hence, it follows that $C_{\boldsymbol{qkp}}^{s_q,s_k,s_p} = 0$ whenever $\cos\theta_q = 0$ and $\cos\theta_k \neq 0$.

The same result can be derived directly, but perhaps less intuitively, from the formula (A 1). If (s_q, s_k, s_p) are a 'fast-slow-fast' resonant triad, then $\cos\theta_q = 0$ and, from the resonance condition (A 7), $s_k = s_p$, $p = k$, $\cos\theta_k = -\cos\theta_p$. Thus, the rate of energy transfer into $\boldsymbol{q}$ disappears because

$$C_{\boldsymbol{qkp}}^{s_q,s_k,s_p} = \tfrac{1}{2}(s_k k - s_p p)\boldsymbol{h}_{s_k}^* \times \boldsymbol{h}_{s_p}^* \cdot \boldsymbol{h}_{s_q}^* = 0. \tag{A 8}$$

On the other hand, the rates of the energy transfer into $\boldsymbol{k}$ and $\boldsymbol{p}$ have the opposite sign since, from (A 2),

$$C_{\boldsymbol{kpq}}^{s_k,s_p,s_q} = -C_{\boldsymbol{pqk}}^{s_p,s_q,s_k}, \tag{A 9}$$

implying that energy only exchanges between the three-dimensional modes through the two-dimensional mode, which acts as a catalyst.

Appendix B. Dynamic Taylor–Proudman Theorem

Here, we use the helical decomposition to give a simpler and self-contained derivation of the Dynamic Taylor–Proudman Theorem for the 'slow-slow-slow' resonant triadic interactions. In a triad consisting of all slow modes $\boldsymbol{k}$, $\boldsymbol{p}$ and $\boldsymbol{q}$, then $k_z = 0$, $p_z = 0$ and $q_z = 0$. In the $k_z = 0$ plane or two-dimensional plane, the wavenumber vector $\boldsymbol{k} = k_x\hat{\boldsymbol{x}} + k_y\hat{\boldsymbol{y}}$ and its amplitude $k = \sqrt{k_x^2 + k_y^2}$. By choosing the helical modes $\boldsymbol{h}_s(\boldsymbol{k}) = \boldsymbol{N} \times \hat{\boldsymbol{k}} + \mathrm{i}s\boldsymbol{v}$ which satisfy $\mathrm{i}\boldsymbol{k} \times \boldsymbol{h}_\pm = \pm|\boldsymbol{k}|\boldsymbol{h}_\pm$ (Waleffe 1992), we have

$$\boldsymbol{h}_s(\boldsymbol{k}) = \hat{\boldsymbol{z}} + \mathrm{i}s\frac{k_y\hat{\boldsymbol{x}} - k_x\hat{\boldsymbol{y}}}{k} = \hat{\boldsymbol{z}} + \mathrm{i}s\hat{\boldsymbol{k}}^\perp. \tag{B 1}$$

Here $\boldsymbol{N} = \boldsymbol{k} \times \hat{\boldsymbol{z}}/|\boldsymbol{k} \times \hat{\boldsymbol{z}}|$ and $\hat{\boldsymbol{k}}^\perp = (k_y\hat{\boldsymbol{x}} - k_x\hat{\boldsymbol{y}})/k$ are unit vectors orthogonal to the unit vector $\hat{\boldsymbol{k}} = \boldsymbol{k}/k$. The other two helical modes in the triad are $\boldsymbol{h}_s(\boldsymbol{p}) = \hat{\boldsymbol{z}} + \mathrm{i}s\hat{\boldsymbol{p}}^\perp$ and $\boldsymbol{h}_s(\boldsymbol{q}) = \hat{\boldsymbol{z}} + \mathrm{i}s\hat{\boldsymbol{q}}^\perp$, where the unit vectors $\hat{\boldsymbol{p}}^\perp = (p_y\hat{\boldsymbol{x}} - p_x\hat{\boldsymbol{y}}/p$ and $\hat{\boldsymbol{q}}^\perp = (q_y\hat{\boldsymbol{x}} - q_x\hat{\boldsymbol{y}})/q$ are perpendicular to the unit wave vectors $\hat{\boldsymbol{p}} = \boldsymbol{p}/p$ and $\hat{\boldsymbol{q}} = \boldsymbol{q}/q$, respectively. The velocity projection onto $\boldsymbol{h}_s$ is

$$\begin{aligned} a_s(k_x, k_y, 0, t) &= \frac{\boldsymbol{h}_s(k_x, k_y, 0) \cdot \hat{\boldsymbol{u}}(k_x, k_y, 0)}{2} \\ &= \tfrac{1}{2}\left[\hat{u}_z(k_x, k_y, 0) + \mathrm{i}s\left(\frac{\hat{u}_x k_y}{k} - \frac{\hat{u}_y k_x}{k}\right)\right]. \end{aligned} \tag{B 2}$$

Since

$$\hat{\boldsymbol{\omega}} = \mathrm{i}\boldsymbol{k} \times \hat{\boldsymbol{u}} = \mathrm{i}(k_x\hat{\boldsymbol{x}} + k_y\hat{\boldsymbol{y}}) \times (\hat{u}_x\hat{\boldsymbol{x}} + \hat{u}_y\hat{\boldsymbol{y}} + \hat{u}_z\hat{\boldsymbol{z}}) = \mathrm{i}(k_x\hat{u}_y - k_y\hat{u}_x)\hat{\boldsymbol{z}} = \hat{\omega}_z\hat{\boldsymbol{z}}, \tag{B 3}$$

(B 2) can be also written as

$$a_s(k_x, k_y, 0, t) = \tfrac{1}{2}\hat{u}_z(k_x, k_y, 0) + \frac{s}{2}\frac{\hat{\omega}_z(k_x, k_y, 0)}{k}. \tag{B 4}$$

Thus, the vertically averaged vertical velocity and the vorticity can be separated from the above equation as

$$\hat{u}_z = a_+ + a_-, \quad \hat{\omega}_z = k(a_+ - a_-). \tag{B 5}$$

For the slow modes $a_{s_k}(t) = A_{s_k}(t)$, the 'averaged equation' (2.8) becomes

$$\left(\partial_t + \frac{1}{Re}k^2\right)a_{s_k} = \frac{1}{4}\sum_{\boldsymbol{k}+\boldsymbol{p}+\boldsymbol{q}=0}\sum_{s_p,s_q}(s_p p - s_q q)\left(\boldsymbol{h}^*_{s_p}\times\boldsymbol{h}^*_{s_q}\right)\cdot\boldsymbol{h}^*_{s_k}a^*_{s_p}a^*_{s_q}. \tag{B 6}$$

Since $\hat{\boldsymbol{p}}^\perp\times\hat{\boldsymbol{q}}^\perp = \hat{\boldsymbol{p}}\times\hat{\boldsymbol{q}}$,

$$\begin{aligned}\left(\boldsymbol{h}^*_{s_p}\times\boldsymbol{h}^*_{s_q}\right)\cdot\boldsymbol{h}^*_{s_k} &= (\hat{\boldsymbol{z}} - \mathrm{i}s\,\hat{\boldsymbol{p}}^\perp)\times(\hat{\boldsymbol{z}} - \mathrm{i}s\hat{\boldsymbol{q}}^\perp)\cdot(\hat{\boldsymbol{z}} - \mathrm{i}s\hat{\boldsymbol{k}}^\perp)\\ &= (s_p\hat{\boldsymbol{p}} - s_k\hat{\boldsymbol{k}})\times(s_k\hat{\boldsymbol{k}} - s_q\hat{\boldsymbol{q}})\cdot\hat{\boldsymbol{z}}.\end{aligned} \tag{B 7}$$

Then, (B 6) becomes

$$\left(\partial_t + \frac{1}{Re}\,k^2\right)a_{s_k} = \frac{1}{4}\sum_{\boldsymbol{k}+\boldsymbol{p}+\boldsymbol{q}=0}\sum_{s_p,s_q}(s_p p - s_q q)(s_p\hat{\boldsymbol{p}} - s_k\hat{\boldsymbol{k}})\times(s_k\hat{\boldsymbol{k}} - s_q\hat{\boldsymbol{q}})\cdot\hat{\boldsymbol{z}}. \tag{B 8}$$

To construct $\hat{u}_z$ and $\hat{\omega}_z$ (equation (B 5)) from the above equation, we have

$$\begin{aligned}&\left(\partial_t + \frac{1}{Re}k^2\right)(a_{+_k} - a_{-_k})\\ &\quad= \frac{1}{2}\sum_{\boldsymbol{k}+\boldsymbol{p}+\boldsymbol{q}=0}\frac{p^2 - q^2}{k}(\hat{\boldsymbol{p}}\times\hat{\boldsymbol{q}}\cdot\hat{\boldsymbol{z}})[-a^*_{+_p}a^*_{+_q} - a^*_{-_p}a^*_{-_q} + a^*_{+_p}a^*_{-_q} + a^*_{-_p}a^*_{+_q}],\end{aligned} \tag{B 9}$$

and

$$\begin{aligned}&\left(\partial_t + \frac{1}{Re}k^2\right)(a_{+_k} + a_{-_k})\\ &= \frac{1}{2}\sum_{\boldsymbol{k}+\boldsymbol{p}+\boldsymbol{q}=0}(\hat{\boldsymbol{p}}\times\hat{\boldsymbol{q}}\cdot\hat{\boldsymbol{z}})[(p-q)(-a^*_{+_p}a^*_{+_q} + a^*_{-_p}a^*_{-_q}) + (p+q)(a^*_{+_p}a^*_{-_q} - a^*_{-_p}a^*_{+_q})].\end{aligned} \tag{B 10}$$

Let $b_k = a_{+_k} - a_{-_k}$ and $\theta_k = a_{+_k} + a_{-_k}$, then $a_{+_k} = (\theta_k + b_k)/2$ and $a_{-_k} = (\theta_k - b_k)/2$. Substituting the above relations into (B 9) and (B 10), we have

$$\left(\partial_t + \frac{1}{Re}\,k^2\right)b_k = -\frac{1}{2}\sum_{\boldsymbol{k}+\boldsymbol{p}+\boldsymbol{q}=0}\frac{p^2 - q^2}{k}\,\hat{\boldsymbol{p}}\times\hat{\boldsymbol{q}}\cdot\hat{\boldsymbol{z}}\;b^*_p b^*_q, \tag{B 11}$$

and

$$\left(\partial_t + \frac{1}{Re}\,k^2\right)\theta_k = \frac{1}{2}\sum_{\boldsymbol{k}+\boldsymbol{p}+\boldsymbol{q}=0}\frac{\hat{\boldsymbol{p}}\times\hat{\boldsymbol{q}}\cdot\hat{\boldsymbol{z}}}{pq}[qb^*_p\theta^*_q - pb^*_q\theta^*_p]. \tag{B 12}$$

Since $\hat{\omega}_z = kb_k$ from (B 5), (B 11) can be written in terms of the vorticity as

$$\left(\partial_t + \frac{1}{Re}\,k^2\right)\hat{\omega}_z = \frac{1}{2}\sum_{\boldsymbol{k}+\boldsymbol{p}+\boldsymbol{q}=0}\frac{\hat{\boldsymbol{p}}\times\hat{\boldsymbol{q}}\cdot\hat{\boldsymbol{z}}}{pq}\left[qb^*_p\hat{\omega}^*_{z_q} - pb^*_q\hat{\omega}^*_{z_p}\right]. \tag{B 13}$$

This is exactly the same as the helical formulation of two-dimensional N-S equation which is given by Waleffe (1993).

Also because of $\hat{u}_z(\boldsymbol{k}) = \theta_k$ from (B 5), (B 12) can be written in terms of $\hat{u}_z(\boldsymbol{k})$ as

$$\left(\partial_t + \frac{1}{Re}\, k^2\right)\hat{u}_{z_k} = \frac{1}{2}\sum_{\boldsymbol{k}+\boldsymbol{p}+\boldsymbol{q}=0} \frac{(\hat{\boldsymbol{p}}\times\hat{\boldsymbol{q}}\cdot\hat{\boldsymbol{z}})}{pq}\left(q b_p^* \hat{u}_{z_q}^* - p b_q^* \hat{u}_{z_p}^*\right). \tag{B 14}$$

This equation has the same structure as the two-dimensional vorticity equation (B 13). It is known that a two-dimensional passive scalar and the two-dimensional vorticity obey homologous equations and, in fact, the above equation is the helical formulation of the two-dimensional passive scalar equation.

Based on the above discussion, we now summarize the Dynamic Taylor–Proudman theorem as the following: in three-dimensional rotating turbulence, when $Ro \to 0$, 'slow-slow-slow' triadic interactions yield the 2D-3C Navier–Stokes equations. Here, 2D-3C refers to two variables (x,y) and three components $(\overline{u}^{3D}, \overline{v}^{3D}, \overline{w}^{3D})$. The vertically averaged horizontal velocity

$$(\overline{u}^{3D}, \overline{v}^{3D}) = \frac{1}{H}\int_0^H (u_x(x, y, z), u_y(x, y, z)\,\mathrm{d}z$$

satisfies the two-dimensional Navier–Stokes equation

$$\partial_t \hat{\omega}_z + \nu k^2 \hat{\omega}_z = -\mathrm{i}k_x \overline{u}^{3D}\widehat{(x, y)\omega_z}(x, y) - \mathrm{i}k_y \overline{v}^{3D}\widehat{(x, y)\omega_z}(x, y), \tag{B 15}$$

and the vertically averaged vertical velocity

$$\overline{w}^{3D} = \frac{1}{H}\int_0^H u_z(x, y, z)\,\mathrm{d}z$$

obeys the two-dimensional passive scalar equation

$$\partial_t \widehat{\overline{w}^{3D}}(\boldsymbol{k}) + \nu k^2 \widehat{\overline{w}^{3D}}(\boldsymbol{k}) = -\mathrm{i}k_x \overline{u}^{3D}\widehat{(x, y)\overline{w}^{3D}}(x, y) - \mathrm{i}k_y \overline{v}^{3D}\widehat{(x, y)\overline{w}^{3D}}(x, y). \tag{B 16}$$

Here, H is the vertical height of the domain and the three averaged velocity components in the Fourier space are as follows:

$$\widehat{\overline{u}^{3D}}(\boldsymbol{k}) = \mathrm{i}\frac{k_y}{k_x^2 + k_y^2}\hat{\omega}_z(\boldsymbol{k}),\ \widehat{\overline{v}^{3D}}(\boldsymbol{k}) = -\mathrm{i}\frac{k_x}{k_x^2 + k_y^2}\hat{\omega}_z(\boldsymbol{k}),\ \widehat{\overline{w}^{3D}}(\boldsymbol{k}) = \hat{u}_z(\boldsymbol{k}). \tag{B 17}$$

REFERENCES

Babin, A., Mahalov, A. & Nicolaenko, B. 1996 Global splitting, integrability and regularity of three-dimensional Euler and Navier–Stokes equations for uniformly rotating fluids. *Eur. J. Mech.*B/*Fluids* **15**, 291–300.

Bardina, J., Ferziger, J. H. & Rogallo, R. S. 1985 Effect of rotation on isotropic turbulence: Computation and modeling. *J. Fluid Mech.* **154**, 321–336.

Bartello, P. 1995 Geostrophic adjustment and inverse cascade in rotating stratified turbulence. *J. Atmos. Sci.* **52**, 4410–4428.

Bartello, P., Métais, O. & Lesieur, M. 1994 Coherent structures in rotating three-dimensional turbulence. *J. Fluid Mech.* **273**, 1–29.

Cambon, C. & Jacquin, L. 1989 Spectral approach to non-isotropic turbulence subjected to rotation. *J. Fluid Mech.* **202**, 295–317.

Cambon, C., Rubinstein, R. & Godeferd, F. S. 2004 Advances in wave turbulence: rapidly rotating flows. *New J. Phys.* **6**, 73.

Celani, A., Lanotte, A., Mazzino, A. & Vergassola, M. 2000 Universality and saturation of intermittency in passive scalar turbulence. *Phys. Rev. Lett.* **84**, 2385–2388.

Craik, A. D. D. 1985 *Wave Interactions and Fluid Flow*. Cambridge University Press.

Embid, P. F. & Majda, A. J. 1996 Averaging over fast gravity waves for geophysics flows with arbitrary potential vorticity. *Commun. Partial Diffl. Equat*. **21**, 619–658.

Embid, P. F. & Majda, A. J. 1998 Low Froude number limiting dynamics for stably stratified flow with small or finite Rossby numbers. *Geophys. Astrophys. Fluid Dyn.* **87**, 1–50.

Greenspan, H. P. 1968 *The Theory of Rotating Fluids*. Cambridge University Press.

Greenspan, H. P. 1969 On the nonlinear interaction of inertial waves. *J. Fluid Mech.* **36**, 257–286.

Holloway, G. 1979 On the spectral evolution of strongly interactive waves. *Geophys. Astrophys. Fluid Dyn.* **11**, 271–287.

Hossain, M. 1994 Reduction in the dimensionality of turbulence due to a strong rotation. *Phys. Fluids* **6**, 1077–1080.

Kraichnan, R. H 1970 Instability in fully developed turbulence. *Phys. Fluids* **13**, 569–575.

Leith, C. E. & Kraichnan, R. H. 1972 Predictability of turbulent flows. *J. Atmos. Sci*. **29**, 1041–1058.

LeLong, P. & Riley, J. J. 1991 Internal wave-vortical mode interactions in strongly stratified flows. *J. Fluid Mech.* **232**, 1–19.

Longuet-Higgins, M. S. & Gill, A. E. 1967 Resonant interactions between planetary waves. *Proc. R. Soc. Lond*. A **299**, 120–140.

Mahalov, A., Nicolaenko, B. & Zhou, Y 1998 Energy spectra of strongly stratified and rotating turbulence. *Phys. Rev.* E **57**, 6187–6190.

Mahalov, A. & Zhou, Y. 1996 Analytical and phenomenological studies of rotating turbulence. *Phys. Fluids* **8**, 2138–2160.

Majda, A. J. & Embid, P. F. 1998 Averaging over fast gravity waves for geophysics flows with unbalanced initial data. *Theor. Comput. Fluid Dyn.* **11**, 155–169.

Mansour, N. N., Cambon, C. & Speziale, C. G. 1992 Theoretical and computational study of rotating isotropic turbulence. In *Studies in Turbulence* (ed. T. B. Gatski, S. Sarkar & C. G. Speziale). Springer.

Newell, A. N. 1969 Rossby wave packet interactions. *J. Fluid Mech.* **35**, 255–271.

Pedlosky, J. 1987 *Geophysical Fluid Dynamics,* 2nd Edn. Springer.

Phillips, O. M. 1960 On the dynamics of unsteady gravity waves of finite amplitude. 1. The elementary interactions. *J. Fluid Mech.* **9**, 193–217.

Phillips, O. M. 1968 The interaction trapping of internal gravity waves. *J. Fluid Mech.* **34**, 407–416.

Phillips, O. M. 1981 Wave interactions – the evolution of an idea. *J. Fluid Mech.* **106**, 215–227.

Siggia, E. D. & Kerr, R. M. 1978 Cascade model of fully developed turbulence. *J. Statist. Phys.* **19**, 543–552.

Smith, L. M. & Waleffe, F. 1999 Transfer of energy to two-dimensional large scales in forced, rotating three-dimensional turbulence. *Phys. Fluids* **6**, 1608–1622.

Smith, L. M. & Yakhot, V. 1993 Bose condensation and small-scale structure generation in a random force driven 2D turbulence. *Phys. Rev. Lett*. **19**, 352–355.

Traugott, S. C. 1958 Influence of solid-body rotation on screen-produced turbulence. *NACA Tech. Note* 4135.

Waleffe, F. 1992 The nature of triad interactions in homogeneous turbulence. *Phys. Fluids* A **4**, 350–363.

Waleffe, F. 1993 Inertial transfers in the helical decomposition. *Phys. Fluids* A **5**, 677–685.

Warn, T. 1986 Statistical mechanical equilibria of the shallow water equations. *Tellus* **38A**, 1–11.

Yeung, P. K. & Zhou, Y. 1998 Numerical study of rotating turbulence with external forcing. *Phys. Fluids* **10**, 2895–2909.